Science
AAAS

Supplementary Materials for

Boom-bust cycles in gray whales associated with dynamic and changing Arctic conditions

Joshua D. Stewart *et al*.

Corresponding author: Joshua D. Stewart, joshua.stewart@oregonstate.edu

Science **382**, 207 (2023)
DOI: 10.1126/science.adi1847

The PDF file includes:

Materials and Methods
Figs. S1 to S9
References

Other Supplementary Material for this manuscript includes the following:

MDAR Reproducibility Checklist

Materials and Methods

Data Sources

Eastern North Pacific gray whales migrate annually from their productive summer feeding grounds in the Arctic to overwintering lagoons on the Baja California peninsula, Mexico, where reproduction occurs and females give birth to calves. For the purposes of our analyses, we assume that the entire population undertakes the annual migration between the Arctic and Mexico each year, although there is a known subpopulation of whales that feed along the Pacific coast of the U.S. and Canada in the summer months, and a number of observations of gray whales outside of their expected seasonal range that challenge this assumption. However, compared to the scale of the entire eastern North Pacific population (~25,000 whales), these subpopulation dynamics (e.g. ~350 whales in the Pacific Coast Feeding Group) most likely do not make a meaningful impact on our model inferences. While the annual migration crosses three countries, most of the survey effort is concentrated in California and along the U.S. west coast as we describe below.

Abundance

The longest-running time series in our analysis is of abundance estimates, generated from counts of southbound gray whales migrating along the U.S. west coast from 1967 – 2022 (*24*, *39*, *40*). Surveys take place from early December to late February at Granite Canyon, in central California, and we consider the index year to be from the January of each survey (i.e. an abundance estimate generated from the December 2019 – February 2020 survey would be considered the 2020 estimate). Southbound migrants are presumed to be adults and juveniles. While females occasionally give birth to calves before reaching Baja California, this is rare and new calves would make a negligible contribution to southbound migration abundance estimates. Counts were not undertaken every year during this period, and the method used to estimate abundance changed in 2006. Abundance estimation from 1967 – 2006 is described in (*41*) whereas the method used from 2006 – 2022 is described in (*40*). We note that both methods were used to generate comparative estimates of abundance in 2006, and while these two estimates were similar, we chose to include them both as observations of total abundance in 2006. Total abundance was estimated each year with uncertainty, and we incorporated this uncertainty into the integrated population model as described below.

Calf Counts

Similar to the total abundance estimates of gray whales, calf production estimates are generated using shore-based counts of northbound migrating female whales with calves. Surveys take place from early March to late May at Piedras Blancas, in central California. Two early estimates of calf production were generated in 1980 and 1981 (*42*), and surveys were conducted continuously from 1994 – 2022 with the exception of 2020, when the survey was halted due to COVID-19 impacts (*25*).

Strandings

Documentation of stranded gray whales in the United States along the west coast of North America are reported opportunistically to the National Oceanic and Atmospheric Administration's National Marine Fisheries Service. For each gray whale stranding reported to the U.S. Marine Mammal Stranding Network, the authorized responding agency is required to complete a Marine Mammal Stranding Report – Level A data form (NOAA Form 89-864; OMB No. 0648-0178; form available at https://www.fisheries.noaa.gov/national/marine-life-distress/level-data-collection-marine-mammal-stranding-events). Level A data include details of each stranding (*e.g.*, species, date, stranding location, carcass condition, sex, length, examiner, signs of human interaction). While reports of stranded whales are recorded from Mexico and Canada, effort and reporting frequency of stranded whales is historically more consistent along the U.S. west coast and Alaska. During periods when an Unusual Mortality Event is declared, additional resources are available to increase survey effort for strandings in Mexico and Canada, but we chose to only include stranding records from the U.S. west coast and Alaska as a data source given the greater consistency in reporting. Within the U.S. Marine Mammal Strandings database, there was a major change to reporting and record keeping of strandings starting in 1990. In addition, survey effort for cetacean strandings in Alaska increased in the early 2000s. We therefore considered counts from 1974 – 1989, 1990 – 2000, and 2001-2022 to be three separate sampling periods as described below. The final U.S. Marine Mammal Stranding data used in this paper were extracted from the database on 05 October 2022 and data through August 31, 2022 are included.

In addition to total strandings numbers, we determined the number of stranded individuals with evidence of human interactions in the form of vessel strike and fishing gear entanglement injuries as recorded in the Level A data. The Findings of Human Interaction data field in the Level A data does not represent cause of stranding or cause of death (https://media.fisheries.noaa.gov/dam-migration/examiners_guide_2023.pdf). The cause of death is only determined for a very small subset of stranded individuals that receive internal examinations or complete necropsies, so confidently assigning an anthropogenic-origin mortality to a stranded whale based upon the presence of anthropogenic injuries listed on the Level A form is not possible. However, we reason that if many more whales are dying as a result of interactions with fishing gear (e.g. due to distributional changes caused by a marine heatwave; Samhouri et al. 2021) or vessel strikes, then proportionally more strandings would have evidence of human interactions. We incorporated counts of stranded gray whales with and without evidence of human interactions in the Level A data into the model as proxies for natural and anthropogenic mortality as described below.

Body Condition

We included two aerial photogrammetry datasets on gray whale body condition in our analyses. The first was collected from fixed wing aircraft along the coast of central California from the Channel Islands in the south to Monterey in the north, as described in Perryman & Lynn (2002). These aerial body condition surveys were conducted both in January, coinciding with the southbound migration, and in March, coinciding with the northbound migration. The survey period spanned 1987 – 2013, although aerial surveys were not conducted every year. The second

body condition dataset was collected using uncrewed aerial systems (drones) at Piedras Blancas during the northbound migration period only, and focused primarily on mother/calf pairs. Drone body condition surveys were conducted from 2015 – 2019, using methods described in (*44*). For our metric of body condition, we used the ratio of the maximum width of a whale to its length. Many recent studies of cetacean body condition have used the ratio of a whale's width at a fixed relative distance along the body to its length as a metric of condition (*18*, *45*, *46*), or more comprehensive indices such as body volume or body area (*47–49*). While these approaches are likely more consistent and therefore preferable to our metric of maximum width divided by length, only length and maximum width measurements were available from the archival fixed-wing photogrammetry datasets of gray whales from 1988-2013 (*26*). For measurements from the drone body condition dataset in 2015-2019, we compared the maximum width to body length ratio with the ratio of width at 50% of the body length to body length, which had a correlation coefficient of 0.77. The body condition metrics calculated using maximum width may be less accurate reflections of nutritive condition than those using width at a fixed relative distance along the body, however given the strong correlation between the two metrics we used the ratio of maximum width to length, allowing us to include body condition metrics from 1988 – 2019 in our analyses. We excluded visibly pregnant females from the dataset as the maximum width of these individuals is likely more closely related to pregnancy-related changes to body shape rather than nutritive condition. In addition, we excluded calves migrating north with their mothers from the body condition dataset, as their condition metrics were likely to be correlated with the condition metrics of their mothers (*48*, *50*), which could confound analyses including those paired samples.

Covariates

We considered three covariates that could potentially explain gray whale population dynamics. Whereas previous studies have evaluated a wide range of environmental variables that could be correlated with gray whale population dynamics (e.g. birth rates; Perryman et al. 2020), we focused on factors that could plausibly have direct causal influences on survival, condition and birth rates. Specifically, we considered metrics of access to Arctic feeding grounds and prey availability at these feeding grounds. While gray whales feed throughout the northern Bering Sea, Chirikov Basin, and Chukchi Sea, our bounding box (Figure S1) covers the region that has historically been a consistent hotspot for observations of foraging gray whales (*12*, *51*). As the Arctic has warmed and remained ice-free for longer, gray whales have expanded their feeding distribution as far north as point Barrow (*12*, *23*). However, the distribution of high-density amphipod prey in these more northerly feeding grounds is far more constrained than in the primary historical gray whale feeding areas between St. Lawrence Island and Point Hope (*12*). Despite a northward expansion, these primary feeding areas in the northern Bering and southern Chukchi sea have remained consistent hotspots for observations of feeding gray whales, with fluctuations in sighting rates that appear to align with benthic prey availability and sea ice cover (*12*, *23*, *51*). We therefore focus on this area for our covariate selection as we posit that it best represents prey availability on key foraging grounds for gray whales, while also providing a consistent long-term time series of in-situ benthic prey collection that spans almost the entire gray whale abundance time series. Within this focal area, we calculated the number of days in each year between the date when sea ice first drops below and first advances past 50% concentration. "Days of open water" was calculated using daily or alternating day sea ice

concentration layers from Sea Ice Index dataset (SII, version 3, ftp://sidads.colorado.edu/DATASETS/NOAA/G02135/north/daily/geotiff/, accessed May 26, 2021) produced by the NOAA National Snow and Ice Data Center (NSIDC) at a nominal resolution of 25 km at 70ºN in polar stereographic projection (EPSG: 3411). Aerial survey counts from the northeast Chukchi Sea indicate that above 50% sea ice concentration gray whale occurrence drops off precipitously, while below this 50% threshold it appears that gray whales can begin to access their summer feeding grounds (*23*). Within the same bounding box we generated an annual index of mean benthic crustacean biomass using in-situ benthic sediment samples collected by the PACMARS and DBO programs between 1970 and 2019 (*28*). Gray whales have been documented feeding on diverse prey assemblages in the Arctic, however their primary prey targets are benthic amphipods and other infaunal crustaceans (*12*). In many of the historically important Arctic gray whale feeding grounds, benthic crustacean abundance has remained stable or increased. However, the species composition has shifted away from the tube building benthic amphipods that are highest in lipid content and therefore highest value prey for gray whales (*12*). As such, we chose to use benthic crustacean biomass (grams of Carbon per cubic meter) as a more direct indicator of benthic prey availability and quality rather than abundance, which may not capture changes in prey quality. Moore et al. (2022) suggest that during periods of potentially low benthic prey availability, gray whales may shift foraging tactics to pelagic habitats, targeting krill and other zooplankton. We therefore included a metric of pelagic zooplankton density from the ECCO Darwin global ocean model (*29*). We used the total density of zooplankton at 5m water depth from the July model time step, within the same bounding box as ice access and benthic crustacean biomass (Figure S1). All covariates were lagged by one year in the model to refer to the prior foraging season. For example, carrying capacity in 2020 was related within the model to the covariate values from summer 2019, which would presumably influence survival, reproduction, and nutritive condition during the following winter and spring. A wider range of lag periods has previously been considered in studies relating gray whale reproductive output to environmental conditions including sea ice extent, and there is biological and empirical support for environmental conditions and feeding opportunities being most relevant during the gestation period (which occurs during the previous summer feeding period), rather than during pre-breeding periods (which would occur at a 2-year lag instead) (*22*).

Integrated Population Model

Process Model

The population dynamics process in our model is described by a discrete logistic growth equation, with a modification such that carrying capacity is variable and indexed by time:

$$N_{t+1} = N_t + rN_t\left(1 - \frac{N_t}{K_t}\right)$$

where N is the model-estimated total abundance of eastern North Pacific gray whales in year t, r is the population's intrinsic maximum growth rate, and K is the carrying capacity in year t. We modified this form of the equation to more easily incorporate births, deaths, and body condition observations:

$$N_{t+1} = N_t * (1 + B_t - M_t)$$

Where *B* is the annual birth rate and *M* is the annual mortality rate in year *t*. Logit-transformed birth rate and nutritive condition were modeled with linear relationships to abundance relative to annual carrying capacity, thus accounting for density dependent effects on vital rates:

$$logit(B_t) = \hat{B} - \beta_B * \frac{N_t}{K_t}$$

And

$$logit(C_t) = \hat{C} - \beta_C * \frac{N_t}{K_t}$$

Where C is the southbound nutritive condition of the population in year *t*, $\hat{B}$ and $\hat{C}$ determine the base birth rate and nutritive condition when abundance is far below carrying capacity, and β is a vector of parameters determining the effects of density dependence on vital rates. Our model tracks mortality from natural and anthropogenic sources separately using a proportional hazards formulation:

$$h_{N,t} = e^{\hat{\gamma}_E + \beta_E * \frac{N_t}{K_t}}$$

And

$$h_{A,t} = e^{\hat{\gamma}_A + \eta_t}$$

And

$$M_t = 1 - e^{-(h_{E,t} + h_{A,t})}$$

Where *h* is the instantaneous hazard rate for either natural mortality *E* or anthropogenic mortality *A* in year *t*, $\hat{\gamma}$ is the base log hazard rate for natural or anthropogenic mortality, β_E is the log hazard ratio associated with a unit increase in population density (relative to annual *K*) and thus determines the strength of density dependent variation in natural mortality, and η is a random effect determining year-to-year variation in anthropogenic hazards. Maximum growth rate *r* from the original logistic equation can then be calculated from the maximum birth rate and minimum mortality rate at low population densities (~ 1% of *K*):

$$logit(B_{max}) = \hat{B} - \beta_B * 0.01$$

and

$$M_{min} = 1 - e^{-e^{\hat{\gamma}_E + \beta_E * 0.01}}$$

And

$$r = B_{max} - M_{min}$$

We set an informative prior distribution for *r* of N[0.1, 0.001], informed by previous estimates of gray whale r_{max} values (*21*).

Annual carrying capacity was estimated as a function of environmental covariates such that:

$$K_t = \widehat{K} * e^{\sum Cov_{c,t} * \beta_c + \epsilon_t}$$

Where K is instantaneous carrying capacity in year t, $\widehat{K}$ is a constant representing the median expected annual K value, Cov_c is Z-scored covariate c (centered and scaled to have mean of 0 and unit variance), β_c is a fitted parameter that determines the effect of covariate c on carrying capacity, and ϵ represents the effect of environmental stochasticity, or unexplained variation in annual K_t, treated as a random normal variable with mean of 0 and standard error of σ_k. We note that missing values of covariates were estimated using auto-regressive techniques, as explained below. We set $\widehat{K}$ = 24,500 based on iteratively re-fitting the model to find the value of $\widehat{K}$ that ensured that expected K_t (calculated from the above equation) was identical to the numerically derived equilibrium abundance calculated by recursively solving the process model with the current values of Cov_c and ϵ until N stabilized (following methods described below in section "Estimating Long term K").

The process model could have been formulated in a variety of ways to explain variability in vital rates and abundance of gray whales. For example, rather than applying covariate effects to explain annual carrying capacity K_t, they could instead be applied to the intrinsic population growth rate parameter r, or to vital rates independently (birth rate, survival rate, nutritive condition) with separately estimated effects. Further, the effects of density dependence could be eliminated altogether by removing carrying capacity from the equation and allowing population fluctuations to be governed entirely by covariates and random effects. However, a preliminary examination of the survey data indicated a significant negative relationship between the log of estimated annual growth rates and abundance (linear model t = 2.492, df=53, p = 0.0159; Figure S9), providing empirical support for density-dependent population dynamics. Annual growth rates also became more variable at higher abundance, with sharp declines of ~10% or more only occurring when the gray whale population was at high abundance levels (Figure S9), suggesting that the magnitude of environmentally-driven booms and busts are density dependent. Most importantly, we believe that modeling covariate effects on K rather than r most closely approximates biological reality. The Bering and Chukchi seas are the primary feeding ground for the vast majority of gray whales (>95%). As such, the conditions in these spatially restricted feeding areas directly impact food availability for almost the entire eastern North Pacific population. We therefore posit that the quality, quantity, and access to that prey will have a greater influence on vital rates when there is high intra-specific competition for limited resources (i.e. at high levels of gray whale abundance). Applying covariate effects to K therefore allows vital rates to be governed by a combination of environmental conditions and intrinsic density dependence, with environmental conditions having a weaker effect on vital rates when gray whale abundance is low.

Observation Model

Observations of annual abundance are included from Granite Canyon survey estimates:

$$n_t \sim Normal[N_t, \sigma_{n_t}]$$

where n is the median or maximum likelihood estimate of abundance in year t, normally distributed around the model-estimated true total abundance with uncertainty σ associated with

each estimate *n* in year *t*, which is either the standard deviation of the posterior distribution for estimates generated using Bayesian methods (*40*) or the standard error of the estimate for those generated using maximum likelihood methods (*39*). Note that Granite Canyon abundance estimates are indexed to year *t* such that the survey period begins in December of year *t-1* and ends in February of year *t* (e.g. the December 2019 – February 2020 survey is considered the abundance estimate for year 2020).

Model estimated annual births *b* are calculated as birth rate *B* multiplied by the annual estimated abundance *N*:

$$b_t = B_t * N_t$$

Empirical estimates of calf production are incorporated into the model as observations of the true number of births:

$$Calves_t \sim Normal[b_t, \sigma_{Calves_t}]$$

where *Calves* refers to the median estimated calf production from Piedras Blancas surveys in year *t*, and σ is the standard deviation of the posterior distribution of each estimate.

The annual number of deaths attributed to natural or anthropogenic mortality is estimated using strandings as a proxy for mortality, such that:

$$Exp.Str_{E,t} = N_t * M_t * \frac{h_{E.t}}{h_{E,t} + h_{A,t}} * P.Str_p$$

and

$$Exp.Str_{A,t} = N_t * M_t * \frac{h_{A.t}}{h_{E,t} + h_{A,t}} * P.Str_p$$

Where *Exp.Str* is the number of dead whales expected to be observed as strandings in year *t* with evidence of human interactions (*A*) or no evidence of human interactions (*E*), which is the product of total mortality *M*, abundance *N*, the proportional contribution to total hazards (*h*) from anthropogenic or natural mortality, and the probability of a dead whale being detected as a stranding in California, Oregon, Washington or Alaska (*P.Str*) during time period *p* associated with year *t*. We included three separate stranding detection periods: 1970-1990, 1990-2000, and 2000-2022 based on expert consultation with NOAA national and regional strandings coordinators as described above. We assume that the probability of a dead whale being detected as a stranding is equal for whales that die of natural causes and those that die of anthropogenic causes, as gray whales have a very near-shore distribution in comparison to other baleen whales. Thus, we do not expect whales that die of anthropogenic causes to be distributed in closer proximity to anthropogenic threats (e.g. coastal vessel traffic and fishing effort) where they may be more likely to wash ashore than those that die of natural causes, which might reasonably create a bias in favor of anthropogenic mortality detection in other species of baleen whale that have more offshore distributions. We used vague prior distributions Beta[1,1] for stranding

proportions *P.Str*. The empirically observed number of strandings *str* with either evidence of human interactions or no evidence of human interactions were assumed to be distributed following a Poisson distribution around the expected number of strandings of each type:

$$str_{E,t} \sim Poisson[Exp.Str_{E,t}]$$

And

$$str_{A,t} \sim Poisson[Exp.Str_{A,t}]$$

In short, there are three model-estimated probabilities of dead whales stranding and being recorded—one for the low-effort survey period pre-1990 and two for the higher effort periods post-1990—that are used to transform observed strandings into overall mortality and thus inform the contributions of density-dependent versus anthropogenic mortality.

We incorporate observations of body condition into the model by assuming that body condition measurements are beta distributed around the mean expected condition during the southbound migration:

$$Cond_{SB,i} \sim Beta[C_t * \tau_{SB}, (1 - C_t) * \tau_{SB}]$$

where *Cond* is the measured body condition of whale *i* in year *t*, *C* is the model-estimated average of southbound condition, and τ_{SB} is the precision parameter of the beta distribution, estimated as part of model fitting. To incorporate northbound body condition measurements, we applied a proportional correction factor to southbound condition *C*, as northbound migrating whales should be in worse condition after fasting for an additional several months:

$$C_{NB,t} = C_t * NB.Adjust$$

And:

$$Cond_{NB,i} \sim Beta[C_{NB,t} * \tau_{NB}, (1 - C_{NB,t}) * \tau_{NB}]$$

Where *NB.Adjust* is a model-estimated correction factor bounded by [0,1], C_{NB} is the population mean northbound condition, and τ_{NB} is the fitted precision parameter of the beta distribution. Note that there are no known repeated measurements for individually identifiable whales, and thus index *i* simply indicates a unique body condition measurement.

Our study period spans 1968 – 2022, but our three candidate Arctic environmental covariates do not span the full study period, and have periodic data gaps. To account for missing data, we fit an auto-regressive random walk process model to the covariate data within the integrated population model to estimate covariate values for data gaps. We assumed that recorded covariate values were perfectly observed, while unobserved covariate values were estimated as:

$$Cov_{C,t} \sim Normal[Cov_{c,t-1}, \sigma_c]$$

where *Cov* is the observed or, for years with no data, model-estimated covariate value at time *t*, for covariate *C*, and σ_C is a fitted parameter specifying process error for covariate *C*. Recorded covariate values were scaled to mean 0 and standard deviation 1 (Z-scored) prior to inclusion in the model, and then during model fitting (after auto-regressive estimation of missing data) were Z-scored a second time. This placed all covariates, including both observed and model-estimated values, on the same scale, thereby making model-estimated coefficients for covariate effects directly comparable. We note that, due to the second Z-scoring step, even observed covariate values had a small amount of variance reflecting variability in the model-estimated values for missing data years.

Estimating Long term K

The annual K_t values can be interpreted as the equilibrium abundance that would eventually be achieved were environmental conditions and stochastic effects to remain indefinitely fixed at the values observed for the current year. However, because environmental conditions are dynamic, we recognize that no single value of annual K_t is representative of average equilibrium abundance over the longer-term. We instead used iterative simulations to calculate long-term *K* as a derived parameter, which we define as the average equilibrium abundance (averaged over a sufficiently long period of time) that would be expected if future variation in environmental conditions and stochastic effects correspond to the observed distributions over the study period. This definition of long-term *K* thus incorporates and accounts for environmental stochasticity.

For each simulation, we randomly sampled a value for each process model parameter from the joint posterior. We then projected the process model forward for 200 years: for each year, we drew random values of each covariate from the empirically derived sampling distributions (which we fit to observed values over the study period), and we drew random values for ϵ from the normal distribution defined by hyperparameter σ_K. The first 100 years of each simulation were used to allow N_t to reach a dynamic equilibrium, and thus discarded, and we saved the average value of N_t over the second 100 years of the simulation. These simulations were repeated 10,000 times, and we used the resulting distribution of average equilibrium abundance values as the posterior distribution of long-term *K*.

Model Fitting

We used vague prior distributions for all model parameters, which we define as weakly informed based on biological feasibility but having no information specific to this analysis. We used Normal[0, 2.5] priors for log-hazard base rate parameters $\hat{\gamma}$ and for logit base parameters $\hat{B}$ and $\hat{C}$. We used Cauchy[0, 2.5] priors for unconstrained β parameters and used half-Cauchy[0, 2.5] priors for β parameters logically constrained to be positive, as well as for variance and precision parameters. We note the Cauchy distribution has been suggested as an effective, uninformative prior because it has a taller peak than the Normal distribution, is leptokurtic ("fat tailed"), and has no defined mean, and thus provides wide potential bounds on parameter space, a tendency to shrink towards 0 for non-significant parameters, and minimized influence of the prior on the estimation of the posterior (*52*). For those parameters constrained to the 0-1 range, we used flat Beta priors with parameters a = b = 1. In the case of initial population size ($N_{t=0}$) we used a weakly informative gamma distribution with shape parameter = 6.75 and rate parameter =

0.0005, as this distribution encompassed a broad range of values consistent with all previously reported historical estimates.

The observed data variables constrained the possible values of unknown parameters in the process model, allowing us to estimate posterior distributions for these parameters using standard Markov Chain Monte Carlo (MCMC) methods. We used R (*53*) and Stan software (*54*) to code and fit the model, saving 20,000 samples after a burn-in of 1000 samples. We evaluated model convergence by graphical examination of trace plots from 20 independent chains and by ensuring that the Gelman-Rubin convergence diagnostic (R-hat) was <1.01 (*55*) and the effective sample size was >500 for all fitted model parameters. We conducted graphical posterior predictive checking to evaluate model goodness of fit, ensuring that out-of-sample predictive distributions of abundance, body condition, calf counts, and stranded carcasses were fully consistent with the equivalent empirical distributions of observed data.

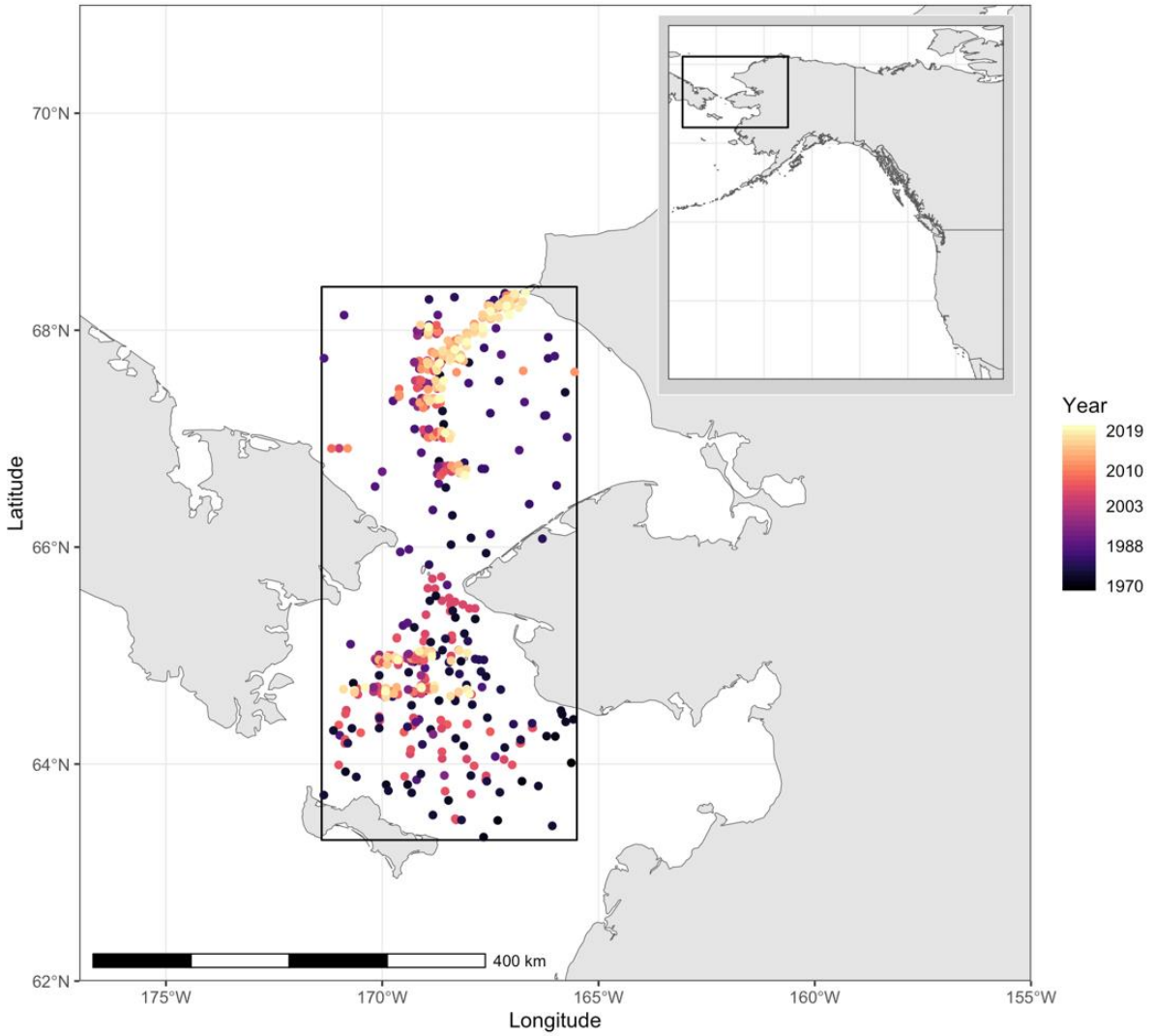

Figure S1: Map of Arctic environmental covariate survey areas and primary gray whale feeding areas in the Bering and Chukchi seas. The black box in the main panel indicates the bounding box for all covariates, including benthic crustacean biomass (plotted), number of days of ice access, and average zooplankton density. Benthic infaunal sampling locations are shown from sampling sites within the bounding box, with color representing sampling year. Plotted sampling locations are jittered for visibility, as many locations had repeated sampling across years. Black box in the inset map indicates the primary map area.

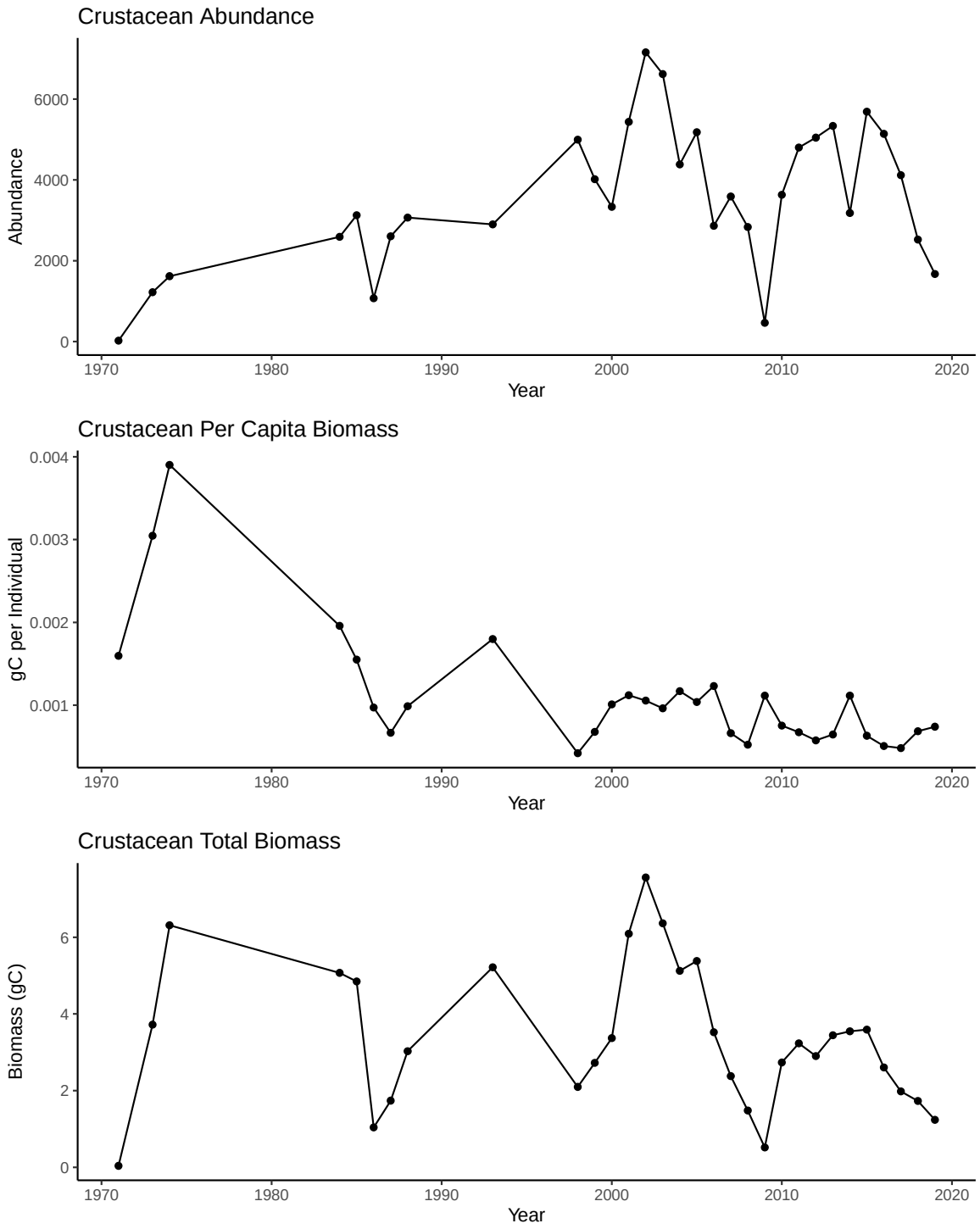

Figure S2: Infaunal benthic crustacean time series from gray whale feeding hotspots in the Bering and Chukchi seas. Top: mean crustacean abundance per sample within the study area. Middle: mean crustacean abundance per sample divided by mean crustacean biomass per sample. Bottom: mean crustacean biomass in grams of carbon per sample.

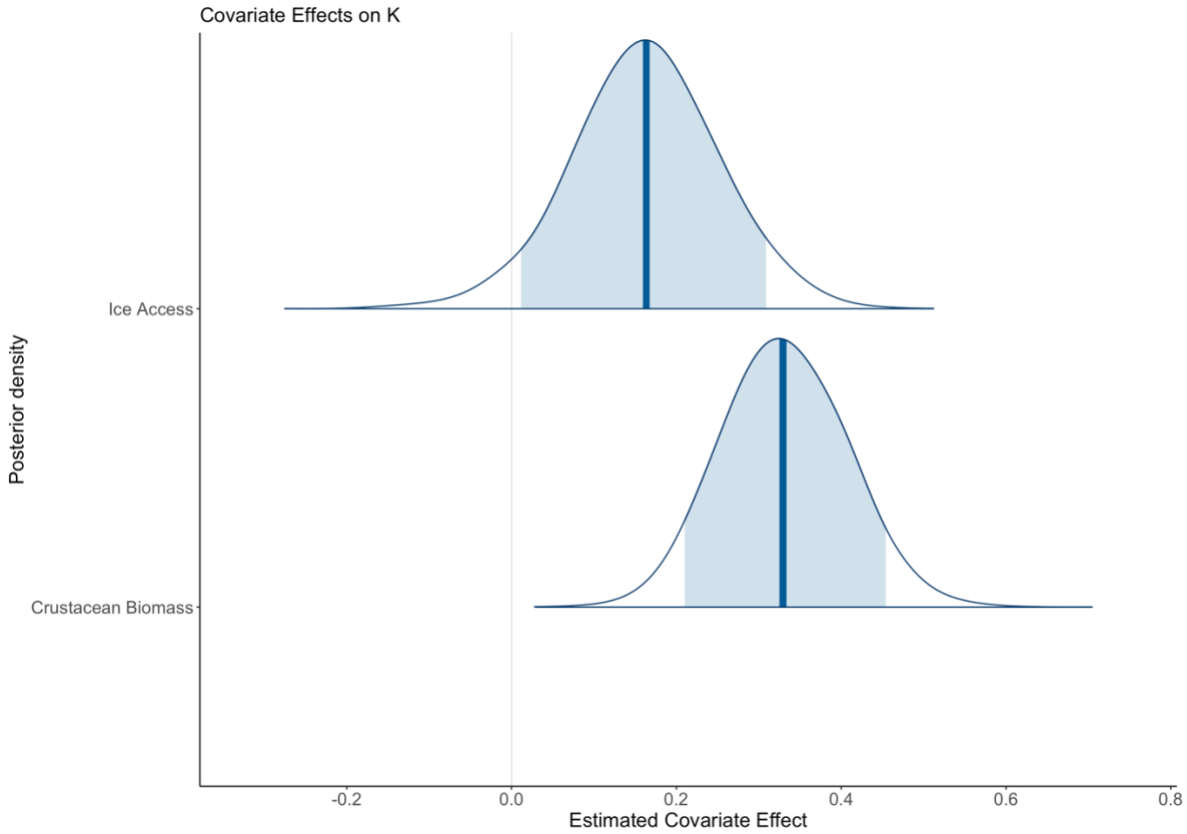

Figure S3: Posterior distributions of covariate effects on annual carrying capacity, for the model formulation with crustacean biomass and ice access. Vertical blue bars indicate the median, and light blue polygons the 90% highest posterior density intervals of the posterior distributions.

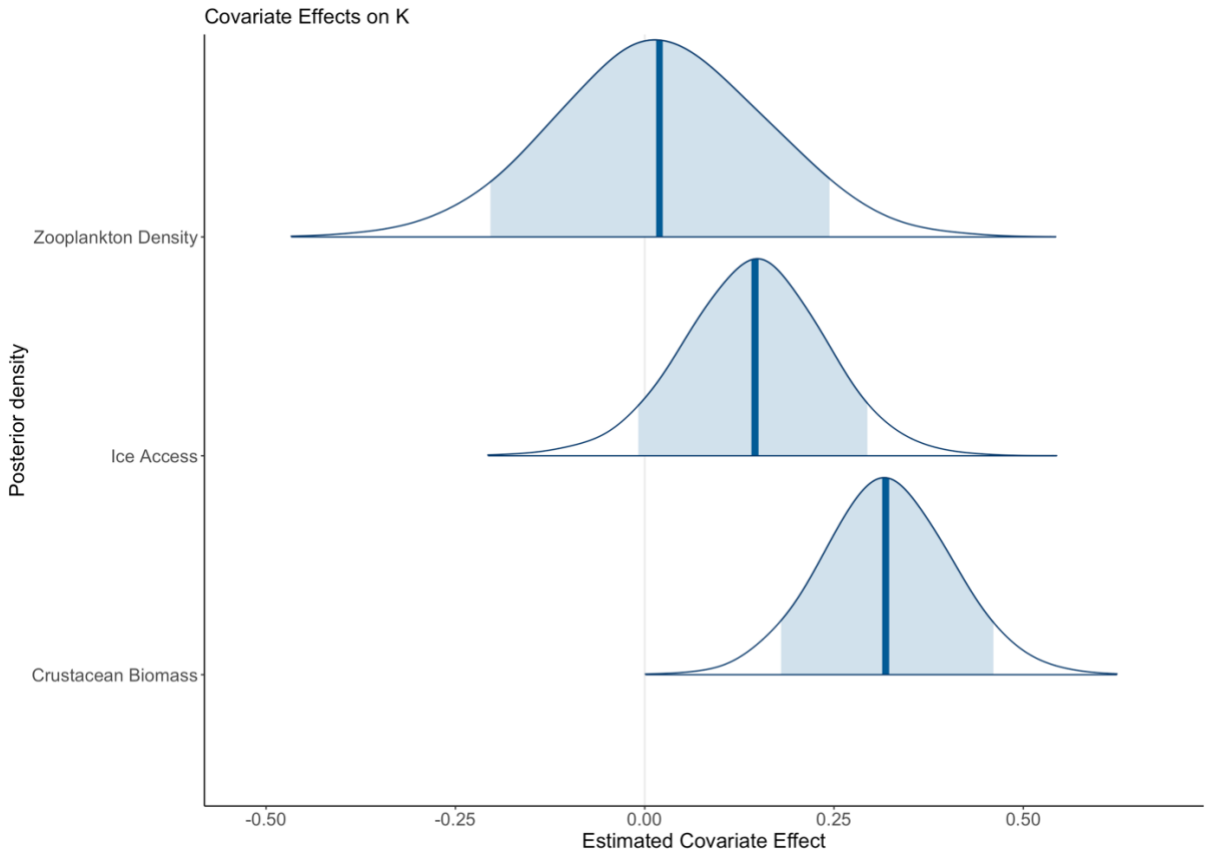

Figure S4: Posterior distributions of covariate effects on annual carrying capacity, for the model formulation with crustacean biomass, ice access, and zooplankton density. Vertical blue bars indicate the median, and light blue polygons the 90% highest posterior density intervals of the posterior distributions.

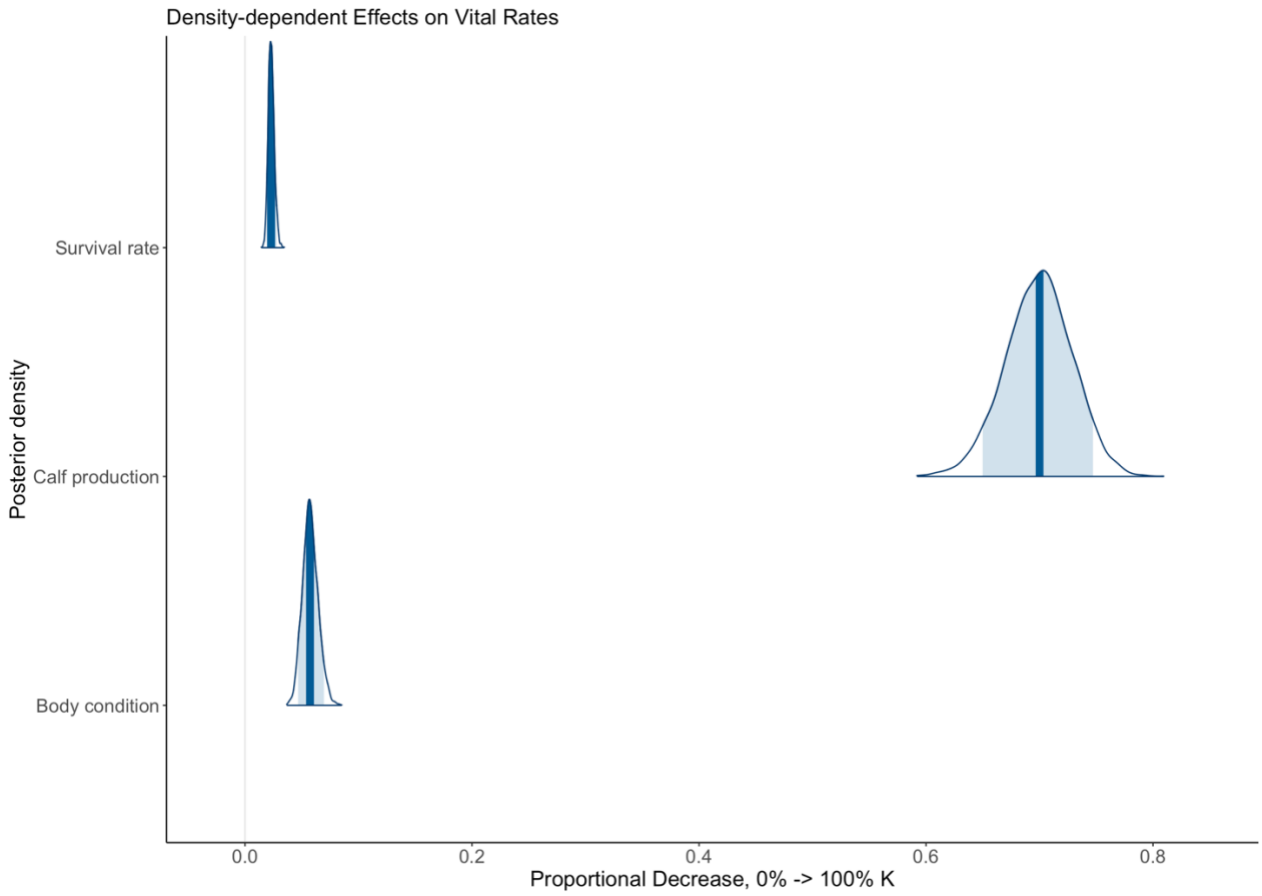

Figure S5: Standardized density-dependent effects on vital rates. Proportional decrease in vital rates over a change in annual abundance (N) relative to annual carrying capacity (K) from N/K = 0 to N/K = 1. Vertical blue bars indicate the median, and light blue polygons the 90% highest posterior density intervals of the posterior distributions.

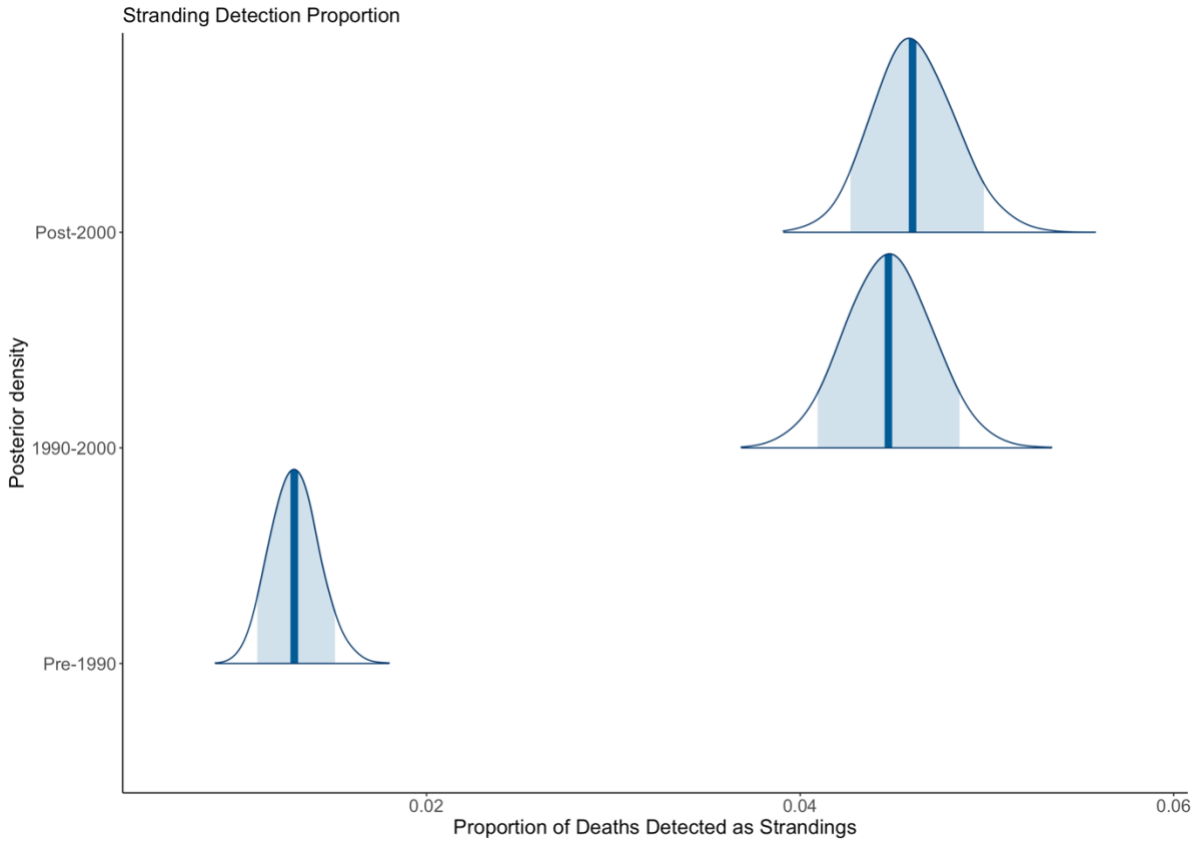

Figure S6: Model-estimated proportion of deaths recovered as strandings for the three stranding detection periods 1970-1990, 1990-2000, and 2000-2022. Vertical blue bars indicate the median, and light blue polygons the 90% highest posterior density intervals of the posterior distributions.

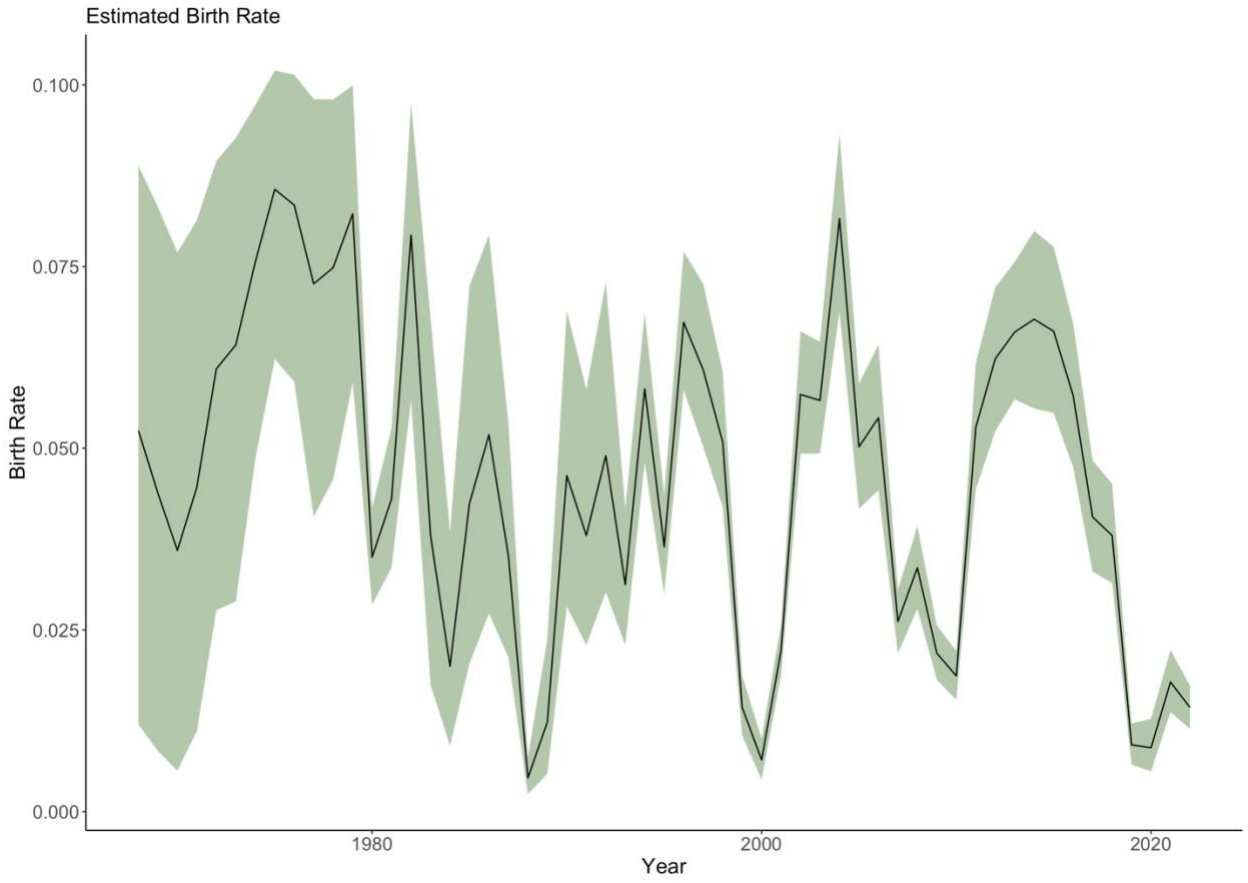

Figure S7: Model-estimated birth rates. The black line indicates the annual median model-estimated birth rate, and the green ribbon indicates the 95% credible intervals of the posterior estimate. Estimates of annual calf production (not shown), which were included as observations of births in the population dynamics model, were available in 1980-81, 1994-2019, and 2021-22.

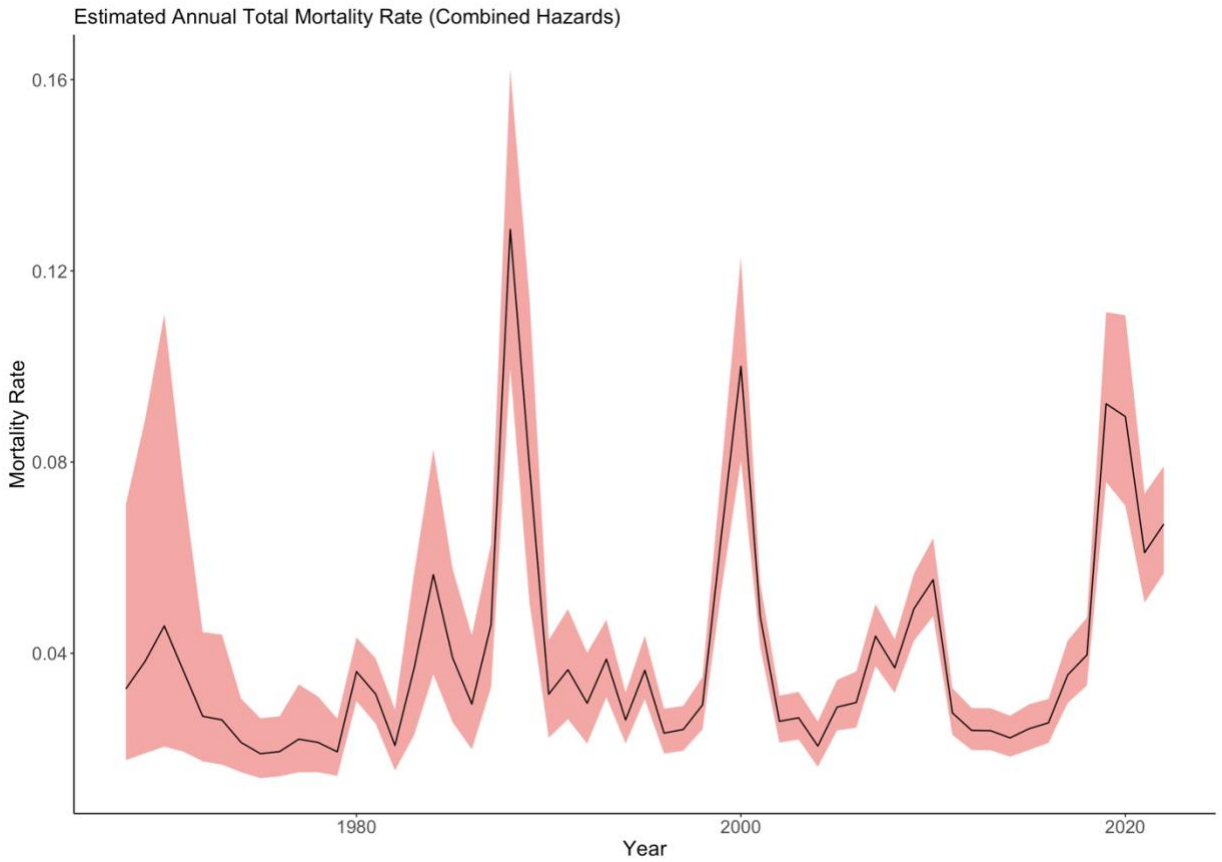

Figure S8: Model-estimated mortality rates. The black line indicates the annual median model-estimated mortality rate (combined anthropogenic and natural hazards), and the green ribbon indicates the 95% credible intervals of the posterior estimate.

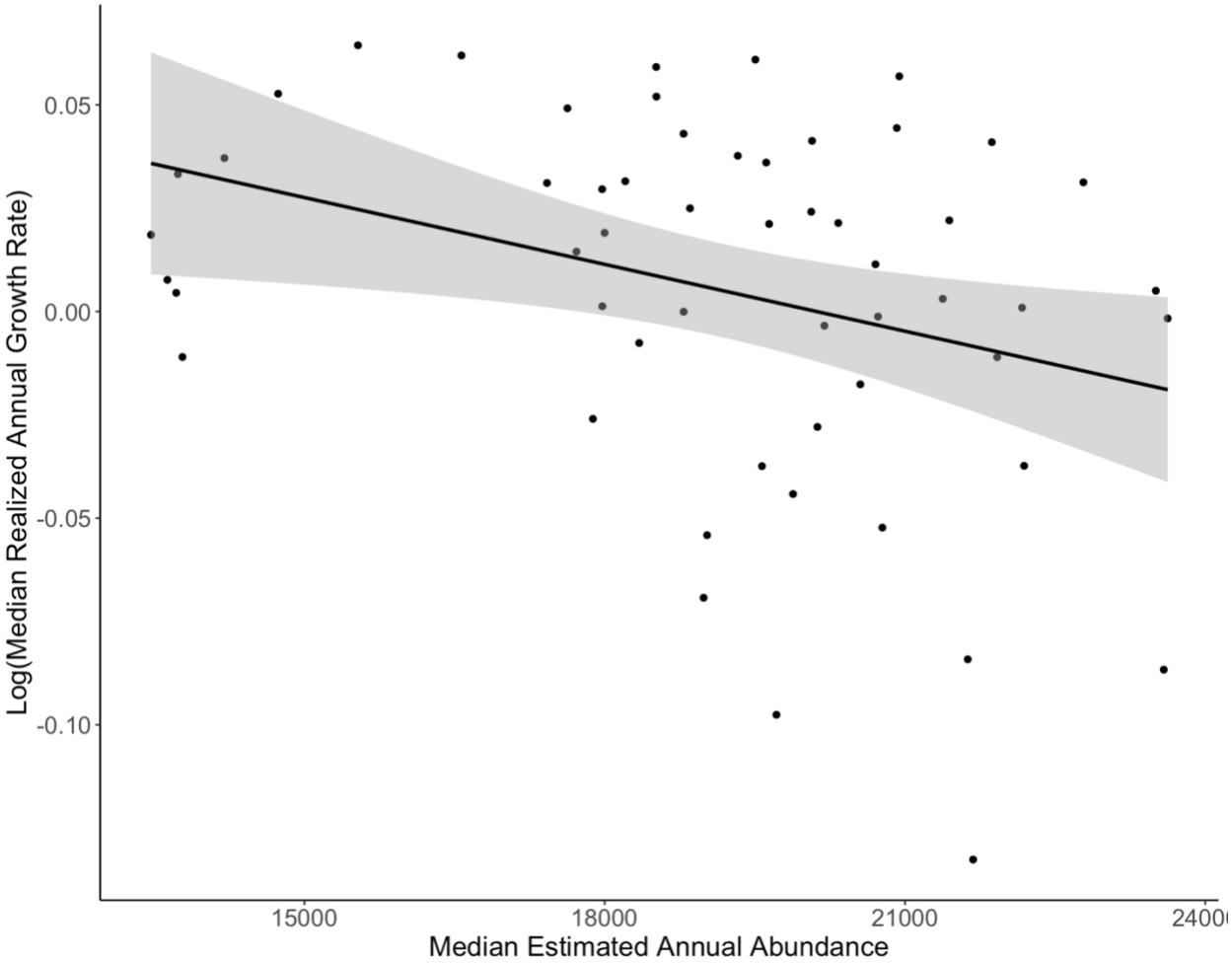

Figure S9. Density-dependent effects on population growth rates. The y-axis represents the log of the median realized annual growth rates (i.e. N_{t+1} / N_t, often represented by λ). Values below zero indicate population decline whereas those above 0 indicate growth. The x-axis represents the annual abundance of the population (N_t). The black line is a simple linear regression with confidence intervals plotted as the gray polygon. The more extreme negative growth rates at greater abundance levels indicate interactive effects of environmental conditions and intra-specific competition.

References and Notes

1. R. C. Highsmith, K. O. Coyle, High productivity of northern Bering Sea benthic amphipods. *Nature* **344**, 862–864 (1990).

2. A. M. Springer, C. P. McRoy, M. Flint, The Bering Sea Green Belt: Shelf-edge processes and ecosystem production. *Fish. Oceanogr.* **5**, 205–223 (1996).

3. J. M. Grebmeier, L. W. Cooper, H. M. Feder, B. I. Sirenko, Ecosystem dynamics of the Pacific-influenced Northern Bering and Chukchi Seas in the Amerasian Arctic. *Prog. Oceanogr.* **71**, 331–361 (2006).

4. K. J. Kuletz, M. C. Ferguson, B. Hurley, A. E. Gall, E. A. Labunski, T. C. Morgan, Seasonal spatial patterns in seabird and marine mammal distribution in the eastern Chukchi and western Beaufort seas: Identifying biologically important pelagic areas. *Prog. Oceanogr.* **136**, 175–200 (2015).

5. J. M. Grebmeier, J. E. Overland, S. E. Moore, E. V. Farley, E. C. Carmack, L. W. Cooper, K. E. Frey, J. H. Helle, F. A. McLaughlin, S. L. McNutt, A major ecosystem shift in the northern Bering Sea. *Science* **311**, 1461–1464 (2006).

6. H. P. Huntington, S. L. Danielson, F. K. Wiese, M. Baker, P. Boveng, J. J. Citta, A. De Robertis, D. M. S. Dickson, E. Farley, J. C. George, K. Iken, D. G. Kimmel, K. Kuletz, C. Ladd, R. Levine, L. Quakenbush, P. Stabeno, K. M. Stafford, D. Stockwell, C. Wilson, Evidence suggests potential transformation of the Pacific Arctic ecosystem is underway. *Nat. Clim. Chang.* **10**, 342–348 (2020).

7. K. R. Arrigo, G. L. van Dijken, Continued increases in Arctic Ocean primary production. *Prog. Oceanogr.* **136**, 60–70 (2015).

8. K. M. Lewis, G. L. van Dijken, K. R. Arrigo, Changes in phytoplankton concentration now drive increased Arctic Ocean primary production. *Science* **369**, 198–202 (2020).

9. J. M. Grebmeier, K. E. Frey, L. W. Cooper, M. Kędra, Trends in benthic macrofaunal populations, seasonal sea ice persistence, and bottom water temperatures in the Bering Strait region. *Oceanography* **31**, 136–151 (2018).

10. J. M. Grebmeier, S. E. Moore, J. E. Overland, K. E. Frey, R. Gradinger, Biological response to recent Pacific Arctic sea ice retreats. *Eos* **91**, 161–162 (2010).

11. G. C. Pike, Migration and feeding of the gray whale (*Eschrichtius gibbosus*). *J. Fish. Res. Board Can.* **19**, 815–838 (1962).

12. S. E. Moore, J. T. Clarke, S. R. Okkonen, J. M. Grebmeier, C. L. Berchok, K. M. Stafford, Changes in gray whale phenology and distribution related to prey variability and ocean biophysics in the northern Bering and eastern Chukchi seas. *PLOS ONE* **17**, e0265934 (2022).

13. A. E. Punt, C. Allison, G. Fay, An examination of assessment models for the eastern North Pacific gray whale based on inertial dynamics. *J. Cetacean Res. Manag.* **6**, 121–132 (2004).

14. S. E. Alter, E. Rynes, S. R. Palumbi, DNA evidence for historic population size and past ecosystem impacts of gray whales. *Proc. Natl. Acad. Sci. U.S.A.* **104**, 15162–15167 (2007).

15. N. D. Pyenson, D. R. Lindberg, What happened to gray whales during the Pleistocene? The ecological impact of sea-level change on benthic feeding areas in the North Pacific Ocean. *PLOS ONE* **6**, e21295 (2011).

16. P. J. Clapham, S. B. Young, R. L. Brownell, Baleen whales: Conservation issues and the status of the most endangered populations. *Mammal Rev.* **29**, 37–62 (1999).

17. B. J. Le Boeuf, H. Pérez-Cortés M., J. Urbán R., B. R. Mate, F. Ollervides U., High gray whale mortality and low recruitment in 1999: Potential causes and implications. (*Eschrichtius robustus*). *J. Cetacean Res. Manag.* **2**, 85–99 (2000).

18. F. Christiansen, F. Rodríguez-González, S. Martínez-Aguilar, J. Urbán, S. Swartz, H. Warick, F. Vivier, L. Bejder, Poor body condition associated with an unusual mortality event in gray whales. *Mar. Ecol. Prog. Ser.* **658**, 237–252 (2020).

19. S. E. Moore, R. Jorge Urbán, W. L. Perryman, F. Gulland, M. Hector Perez-Cortes, P. R. Wade, L. Rojas-Bracho, T. Rowles, Are gray whales hitting "K" hard? *Mar. Mamm. Sci.* **17**, 954–958 (2001).

20. J. R. Brandon, A. E. Punt, "Assessment of the eastern stock of North Pacific gray whales: incorporating calf production, sea-ice and strandings data," paper SC/61/AWMP2 presented to the International Whaling Commission (IWC) Scientific Committee (2009).

21. A. E. Punt, P. R. Wade, "Population status of the eastern North Pacific stock of gray whales in 2009," US Department of Commerce, National Oceanic and Atmospheric Administration (NOAA) Technical Memo NMFS-AFSC-207, 43 (2009).

22. W. L. Perryman, T. Joyce, D. W. Weller, J. W. Durban, Environmental factors influencing eastern North Pacific gray whale calf production 1994–2016. *Mar. Mamm. Sci.* **37**, 448–462 (2020).

23. T. W. Joyce, M. C. Ferguson, C. L. Berchok, D. L. Wright, J. L. Crance, E. K. Braen, T. Eguchi, W. L. Perryman, D. W. Weller, The role of sea ice in the distribution, habitat use, and phenology of eastern North Pacific gray whales. *Mar. Ecol. Prog. Ser.* **709**, 141–158 (2023).

24. T. Eguchi, A. R. Lang, D. W. Weller, "Abundance and migratory phenology of Eastern North Pacific gray whales 2021/2022," US Department of Commerce, NOAA Technical Memorandum NMFS-SWFSC-668 (2022); .

25. T. Eguchi, A. R. Lang, D. W. Weller, "Eastern North Pacific gray whale calf production 1994-2022," US Department of Commerce, NOAA Technical Memorandum NMFS-SWFSC-667 (2022); .

26. W. L. Perryman, M. S. Lynn, Evaluation of nutritive condition and reproductive status of migrating gray whales (*Eschrichtius robustus*) based on analysis of photogrammetric data. *J. Cetacean Res. Manag.* **4**, 155–164 (2002).

27. G. Gailey, O. Sychenko, O. Tyurneva, Y. Yakovlev, V. Vertyankin, P. van der Wolf, K. Drozdov, I. Zhmaev, Effects of sea ice on growth rates of an endangered population of gray whales. *Sci. Rep.* **10**, 1553 (2020).

28. J. M. Grebmeier, L. W. Cooper, Benthic macroinfaunal and dominant taxa samples collected from Northern Bering Sea to Chukchi Sea, 1970–2019 (2023); https://arcticdata.io/catalog/view/doi%3A10.18739%2FA24T6F480.

29. D. Carroll, D. Menemenlis, J. F. Adkins, K. W. Bowman, H. Brix, S. Dutkiewicz, I. Fenty, M. M. Gierach, C. Hill, O. Jahn, P. Landschützer, J. M. Lauderdale, J. Liu, M. Manizza, J. D. Naviaux, C. Rödenbeck, D. S. Schimel, T. Van der Stocken, H. Zhang, The ECCO-Darwin Data-Assimilative Global Ocean Biogeochemistry Model: Estimates of seasonal to multidecadal surface ocean pCO_2 and air-sea CO_2 Flux. *J. Adv. Model. Earth Syst.* **12**, e2019MS001888 (2020).

30. R. C. Lewontin, D. Cohen, On population growth in a randomly varying environment. *Proc. Natl. Acad. Sci. U.S.A.* **62**, 1056–1060 (1969).

31. J. Roughgarden, A simple model for population dynamics in stochastic environments. *Am. Nat.* **109**, 713–736 (1975).

32. D. G. Heckel, J. Roughgarden, A species near its equilibrium size in a fluctuating environment can evolve a lower intrinsic rate of increase. *Proc. Natl. Acad. Sci. U.S.A.* **77**, 7497–7500 (1980).

33. C. Scott Baker, P. J. Clapham, Modelling the past and future of whales and whaling. *Trends Ecol. Evol.* **19**, 365–371 (2004).

34. V. J. D. Tulloch, É. E. Plagányi, C. Brown, A. J. Richardson, R. Matear, Future recovery of baleen whales is imperiled by climate change. *Glob. Change Biol.* **25**, 1263–1281 (2019).

35. M. S. Savoca, M. F. Czapanskiy, S. R. Kahane-Rapport, W. T. Gough, J. A. Fahlbusch, K. C. Bierlich, P. S. Segre, J. Di Clemente, G. S. Penry, D. N. Wiley, J. Calambokidis, D. P. Nowacek, D. W. Johnston, N. D. Pyenson, A. S. Friedlaender, E. L. Hazen, J. A. Goldbogen, Baleen whale prey consumption based on high-resolution foraging measurements. *Nature* **599**, 85–90 (2021).

36. O. Hoegh-Guldberg, J. F. Bruno, The impact of climate change on the world's marine ecosystems. *Science* **328**, 1523–1528 (2010).

37. G. C. Hays, A. J. Richardson, C. Robinson, Climate change and marine plankton. *Trends Ecol. Evol.* **20**, 337–344 (2005).

38. J. D. Stewart *et al*., stewart6/ENPGW-IPM: Data and Code for Stewart et al. Boom-bust cycles in gray whales. Zenodo (2023); https://doi.org/10.5281/zenodo.8201214.

39. J. L. Laake, A. E. Punt, Gray whale southbound migration surveys 1967–2006: An integrated re-analysis. *J. Cetacean Res. Manag.* **12**, 287–306 (2012).

40. J. W. Durban, D. W. Weller, A. R. Lang, W. L. Perryman, Estimating gray whale abundance from shore-based Counts using a multilevel Bayesian model. *J. Cetacean Res. Manag.* **15**, 61–68 (2015).

41. J. Laake, A. Punt, R. Hobbs, M. Ferguson, D. Rugh, J. Breiwick, “Re-analysis of Gray Whale 1967-2006,” NOAA Technical Memoradum NMFS-AFSC-203 (2009).

42. S. L. Swartz, M. L. Jones, Gray whale (*Eschrichtius robustus*) calf production and mortality in the winter range. *Rep. Int. Whaling Comm.* **34**, 503–507 (1983).

43. J. F. Samhouri, B. E. Feist, M. C. Fisher, O. Liu, S. M. Woodman, B. Abrahms, K. A. Forney, E. L. Hazen, D. Lawson, J. Redfern, L. E. Saez, Marine heatwave challenges solutions to human-wildlife conflict. *Proc. R. Soc. B Biol. Sci.* **288** (2021).

44. J. W. Durban, H. Fearnbach, A. Paredes, L. S. Hickmott, D. J. LeRoi, Size and body condition of sympatric killer whale ecotypes around the Antarctic Peninsula. *Mar. Ecol. Prog. Ser.* **677**, 209–217 (2021).

45. J. W. Durban, M. J. Moore, G. Chiang, L. S. Hickmott, A. Bocconcelli, G. Howes, P. A. Bahamonde, W. L. Perryman, D. J. LeRoi, Photogrammetry of blue whales with an unmanned hexacopter. *Mar. Mamm. Sci.* **32**, 1510–1515 (2016).

46. H. Fearnbach, J. W. Durban, L. G. Barrett-Lennard, D. K. Ellifrit, K. C. Balcomb III, Evaluating the power of photogrammetry for monitoring killer whale body condition. *Mar. Mamm. Sci.* **36**, 359–364 (2020).

47. F. Christiansen, S. Dawson, J. Durban, H. Fearnbach, C. Miller, L. Bejder, M. Uhart, M. Sironi, P. Corkeron, W. Rayment, E. Leunissen, E. Haria, R. Ward, H. Warick, I. Kerr, M. Lynn, H. Pettis, M. Moore, Population comparison of right whale body condition reveals poor state of the North Atlantic right whale. *Mar. Ecol. Prog. Ser.* **640**, 1–16 (2020).

48. F. Christiansen, A. M. Dujon, K. R. Sprogis, J. P. Y. Arnould, L. Bejder, Noninvasive unmanned aerial vehicle provides estimates of the energetic cost of reproduction in humpback whales. *Ecosphere* **7**, 1–18 (2016).

49. L. Soledade Lemos, J. D. Burnett, T. E. Chandler, J. L. Sumich, L. G. Torres, Intra- and inter-annual variation in gray whale body condition on a foraging ground. *Ecosphere* **11**, e03094 (2020).

50. F. Christiansen, F. Vivier, C. Charlton, R. Ward, A. Amerson, S. Burnell, L. Bejder, Maternal body size and condition determine calf growth rates in Southern right whales. *Mar. Ecol. Prog. Ser.* **592**, 267–281 (2018).

51. S. E. Moore, J. M. Grebmeier, J. R. Davies, Gray whale distribution relative to forage habitat in the northern Bering Sea: Current conditions and retrospective summary. *Can. J. Zool.* **81**, 734–742 (2003).

52. A. Gelman, A. Jakulin, M. G. Pittau, Y.-S. Su, A weakly informative default prior distribution for logistic and other regression models. *Ann. Appl. Stat.* **2**, 1360–1383 (2008).

53. R Core Team, R: A language and environment for statistical computing (R Foundation for Statistical Computing, 2021); http://www.r-project.org.

54. Stan Development Team, *Stan Modeling Language Users Guide and Reference Manual*, version 2.31 (2023); https://mc-stan.org.

55. A. Gelman, D. B. Rubin, Inference from iterative simulation using multiple sequences. *Stat. Sci.* **7**, 457–472 (1992).